

# Activation cross-sections of long lived products of deuteron induced nuclear reactions on dysprosium up to 50 MeV

F. Tárkányi<sup>a</sup>, F. Ditrói<sup>a,\*</sup>, S. Takács<sup>a</sup>, J. Csikai<sup>a</sup>, A. Hermanne<sup>b</sup>, A.V. Ignatyuk<sup>c</sup>

<sup>a</sup>*Institute for Nuclear Research of the Hungarian Academy of Sciences (ATOMKI), Debrecen, Hungary*

<sup>b</sup>*Cyclotron Laboratory, Vrije Universiteit Brussel (VUB), Brussels, Belgium*

<sup>c</sup>*Institute of Physics and Power Engineering (IPPE), Obninsk, Russia*

## Abstract

Activation cross-sections for production of  $^{162m,161,155}\text{Ho}$ ,  $^{165,159,157,155}\text{Dy}$  and  $^{161,160,156,155}\text{Tb}$  radionuclides in deuteron induced nuclear reactions on elemental dysprosium were measured up to 50 MeV for practical application and the test of the predictive power of nuclear reaction model codes. A stacked-foil irradiation technique and off-line  $\gamma$ -ray spectrometry were used to determine the activities. No earlier cross-section data were found in the literature. The experimental data are compared with the predictions of the ALICE-D, EMPIRE-D and TALYS codes. Integral production yields were calculated from the fitted experimental data.

**Keywords:** dysprosium target, deuteron irradiation, holmium, dysprosium and terbium radio-isotopes, physical yield

## 1. Introduction

In the frame of our systematic study on the excitation functions of light charged particle induced nuclear reactions, the excitation functions for radionuclides production by deuteron irradiation of natDy were measured. Dysprosium is being a high priority and critical strategic metal now used world-wide for high technology, nuclear, clean energy and military applications. The knowledge on the activation cross-sections for light charged particles (ions) and neutron induced reactions are important for various applications. The elemental dysprosium and some of its radionuclides are known to have applications in fission reactor physics and in medical field. The elemental dysprosium has a high thermal neutron absorption cross-section, which makes it interesting for making neutron-absorbing control rods in nuclear reactors (Kannan and Ganesan, 2010), and a resonance absorber to control the coolant void reactivity in Advanced Heavy Water

Reactor (AHWR) (Kannan and Ganesan, 2010). In medical treating damaged joints, irradiation with  $^{165}\text{Dy}$  has proved to be more effective than traditional surgery (Srivastava, 2004), and  $^{159}\text{Dy}$  has been advocated for transmission imaging and bone mineral analysis (Rao et al., 1977). An alternative production route for radionuclides of lanthanides using high intensity lasers or light sources was studied recently by a group in Grenoble (Habs and Köster, 2012). There were several aims of the study

- The earlier mentioned global task: the systematic study of the deuteron induced activation data, taking into account that no earlier data were found in the literature.
- Investigation of different production routes of the  $^{161}\text{Ho}$  medical radioisotope
- Investigation of the predictive power of widely used theoretical codes, via systematic comparison between the experimental and theoretical data in connection with the FENDL-3 Project (IAEA).
- To get experimental data in a wide mass region for

\*Corresponding author: ditroi@atomki.hu

(d,p) reactions to prepare systematics to be used in upgrading of nuclear reactions models for codes allowing better description of deuteron induced reactions.

Part of the experimental data for production of  $^{161}\text{Ho}$  was published recently (Tarkanyi et al., 2013). Here we repeat the data related to this radionuclide in graphical form for completeness and for comparison with the theories.

## 2. Experiment and data evaluation

The general characteristics and procedures for irradiation, activity assessment and data evaluation (including estimation of uncertainties) were similar to those in our earlier works (Takacs et al., 2011; Tarkanyi et al., 2012). The used high purity target foils (<98% purity) were bought from Goodfellow© and were handled according to the producer's recommendations. The foil thicknesses and homogeneity were accurately re-measured. The main experimental parameters for the present study are summarized in Table 1 (Andersen and Ziegler, 1977; Bonardi, 1987; Canberra, 2000; Kinsey et al., 2010; of-Weights-and Measures, 1993; Pritychenko and Sonzogni, 2003; Székely, 1985; Tarkanyi et al., 1991, 2001) together with the methods used in data evaluation. The used decay data and Q values of the contributing reactions are collected in Table 2. To illustrate the reliability of the incident energy and the intensity of the deuteron beam along the stack, the simultaneously measured complete excitation function of the monitor reaction  $^{27}\text{Al}(d,x)^{24}\text{Na}$  is shown in Fig. 1 in comparison with the recommended data taken from (Tarkanyi et al., 2001).

## 3. Theory

The ALICE-IPPE-D and EMPIRE-D (Dityuk et al., 1998; Herman et al., 2007) calculations were performed using the recommended values for the input parameters. The results of TALYS (Koning et al., 2007) code were taken from the TENDL 2012 library (Koning et al., 2012). The ALICE-D and EMPIRE-D are the modified version of ALICE-IPPE (Dityuk et al., 1998) and EMPIRE (Herman et al., 2007) codes and were developed at IPPE (Institute of Physics and Power Engineering, Obninsk, Russia) for better description of activation cross-sections of

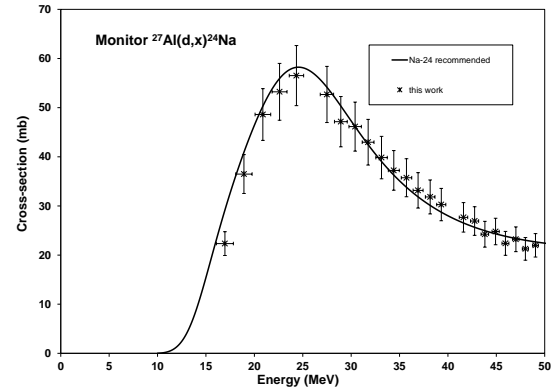


Figure 1: The simultaneously measured monitor reactions for determination of deuteron beam energy and intensity

deuteron induced reactions by using energy dependent enhancement factor (Ignatyuk, 2011) for simulation of direct (d,p) and (d,t) transitions. Independent data for isomers with ALICE-D code was obtained by using the isomeric ratios calculated with EMPIRE-D. Separate sets of calculations were performed for all stable Dy isotopes as target nuclei. The excitation functions for natural isotopic composition were obtained by summing all these individual excitation functions with weight of their respective natural abundances.

## 4. Results

### 4.1. Cross-sections

Activation cross-sections for production of the  $^{162m,161,155}\text{Ho}$ ,  $^{165,159,157,155}\text{Dy}$  and  $^{161,160,156,155}\text{Tb}$  radionuclides were measured. The experimental cross-section data are shown in Figs. 2-11 in comparison with the predictions of theoretical codes. The numerical data are collected in Tables 3 and 4. The cross-section values of holmium production are for direct production via (d,xn) reactions. The dysprosium radio-isotopes are produced directly via (d,pxn) reactions or additionally through the decay of the shorter-lived isobaric parent holmium radioisotope (cumulative cross-section). The terbium radioisotopes are produced directly via (d,2pxn) reaction

Table 1: Main experimental parameters and methods of data evaluation

Parameter	Value	Data evaluation steps	Used method, software, database
Incident particle	Deuteron	Gamma spectra evaluation	Genie 2000 (Canberra, 2000), Forgamma (Székely, 1985)
Measurement method	Stacked foil	Determination of beam intensity	Faraday cup (preliminary) Fitted monitor reaction (final)(Tarkanyi et al., 1991)
Stack composition	Tb-Al-Dy, repeated 15 times	Decay data	NUDAT 2.6 (Kinsey et al., 2010)
Target and thickness	$^{nat}\text{Dy}$ foil, 100.59 $\mu\text{m}$	Reaction Q-values	Q-value calculator (Pritychenko and Sonzogni, 2003)
Number of targetfoils	15 (Dy)	Determination of beam energy	Andersen (preliminary) (Andersen and Ziegler, 1977) Fitted monitor reaction (final) (Tarkanyi et al., 1991)
Accelerator	Cyclone 90 cyclotron of the Université Catholique in Louvain la Neuve (LLN)	Uncertainty of energy	cumulative effects of possible uncertainties
Primary energy	50 MeV	Cross-sections	Elemental cross-section
Irradiation time	30 min	Uncertainty of cross-sections	sum in quadrature of all individual contributions (of-Weights-and Measures, 1993)
Beam current	120 nA	Yield	Physical yield (Bonardi, 1987)
Monitor reaction, [recommended values]	$^{27}\text{Al}(d,x)^{24}\text{Na}$ reaction ((Tarkanyi et al., 2001)		
Monitor target and thickness	$^{nat}\text{Al}$ , 26.96 $\mu\text{m}$		
detector	HpGe		
g-spectra measurements	4 series		
Cooling times	4h, 30h, 430, 2380h		

(including complex particle emission), or additionally from the decay of parent dysprosium or holmium radioisotopes. Taking into account that the contribution from the decay of the holmium radioisotopes is low, these contributions were neglected in the presented theoretical results. The ground-state of the produced radioisotopes out of the direct production can be produced additionally through the internal transition of the isomeric state. The cross-section is marked with (m+), when the half-life of the isomeric state is significantly shorter compared to the half-life of the ground state and the cross-section of the production of ground state were deduced from spectra after nearly complete decay of the isomeric state.

#### 4.1.1. Cross-sections for the $^{nat}\text{Dy}(d,x)^{162m}\text{Ho}$ reaction

The production cross-sections of  $^{162m}\text{Ho}$  ( $T_{1/2}=67.0$  min) are shown in Fig. 2. None of the theoretical calculations represents well the experimental data and large disagreements exist among the codes. TENDL-2012 values, which are the results of most recent version of TALYS are a factor of 2 higher and shifted to higher energies compared to the previous results.

#### 4.1.2. Cross-sections for the $^{nat}\text{Dy}(d,x)^{161g}\text{Ho}(m+)$ reaction

The measured cross-section include the full contribution of the decay of the short-lived isomer ( $T_{1/2} = 6.7$  s). According to Fig. 3, the shape of the experimental and theoretical excitation functions of  $^{161}\text{Ho}$  ( $T_{1/2} = 2.48$  h) are similar, but the overestimation of all codes is surprisingly

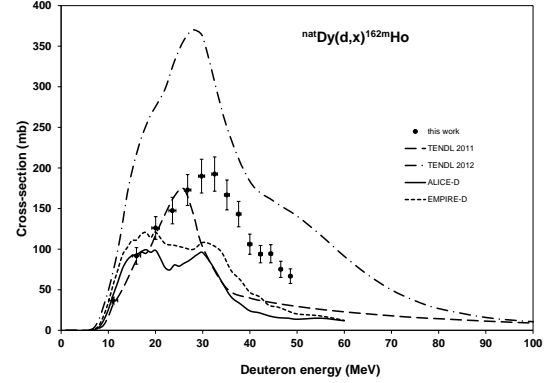


Figure 2: Experimental and theoretical excitation functions for  $^{nat}\text{Dy}(d,x)^{162m}\text{Ho}$

high. For the TENDL results (both libraries give about the same values) a scaling factor of 0.55 results in a reasonable representation of the experiment.

#### 4.1.3. Cross-sections for the $^{nat}\text{Dy}(d,x)^{165g}\text{Dy}(m+)$ reaction

$^{165}\text{Dy}$  ( $T_{1/2} = 2.334$  h) is produced only via the  $^{164}\text{Dy}(d,p)$  reaction. The measured cross-section contains the contribution of the complete decay of the shorter-lived isomeric state ( $T_{1/2}=1.257$  min) that decays with IT

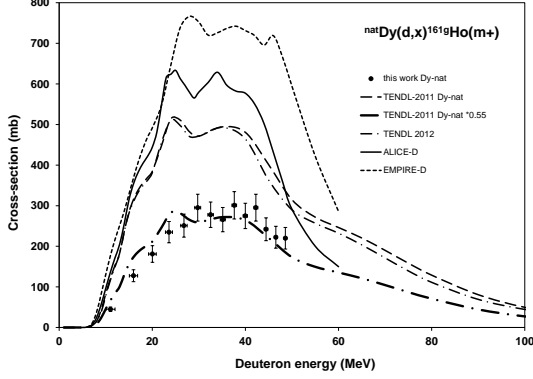


Figure 3: Experimental and theoretical excitation functions for  $^{nat}\text{Dy}(d,x)^{161g}\text{Ho}(m+)$

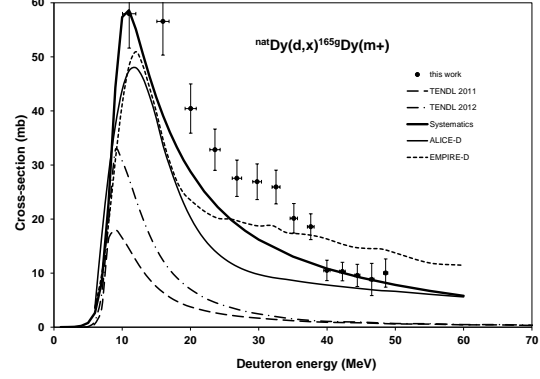


Figure 4: Experimental and theoretical excitation functions for  $^{nat}\text{Dy}(d,x)^{165g}\text{Dy}(m+)$

(97.74 %) to the ground state ( $m+$ ). The experimental data are in good agreement with the systematics of the experimental (d,p) cross-sections above 40 MeV and between the predictions of EMPIRE-D and ALICE-D. The new TENDL 2012 data are closer to the experiment than TENDL 2011 but the underestimation is still significant.

#### 4.1.4. Cross-sections for the $^{nat}\text{Dy}(d,x)^{159}\text{Dy}(cum)$ reaction

The cumulative cross-sections of  $^{159}\text{Dy}$  ( $T_{1/2} = 144.4$  d) include the direct production and the contribution from the decay of  $^{159}\text{Ho}$  ( $T_{1/2} = 33.05$  min), were impossible to measure in our experimental conditions (too long cooling time). The overestimations of the cumulative cross-sections given in both TENDL libraries and by the ALICE-D and EMPIRE-D codes are significant (Fig. 5).

#### 4.1.5. Cross-sections for the $^{nat}\text{Dy}(d,x)^{157}\text{Dy}(cum)$ reaction

Under our experimental circumstances we can deduce only cumulative cross-sections for production of  $^{157}\text{Dy}$  ( $T_{1/2} = 8.14$  h) including the contribution of total decay of short-lived parent  $^{157}\text{Ho}$  ( $T_{1/2} = 12.6$  min). The three codes reproduce well the complex shape of the cumulative experimental excitation function (direct on multiple stable target isotopes at higher energy and parent decay

below 15 MeV) (see Fig. 6), but are one order of magnitude lower for the  $^{156}\text{Dy}(d,n)^{157}\text{Ho}$  reaction. At higher energies all codes overestimate the experimental results by a factor of two. According to the theory the direct reaction contributes only by about 20%.

#### 4.1.6. Cross-sections for the $^{nat}\text{Dy}(d,x)^{155}\text{Dy}(cum)$ reaction

The cumulative cross-section of the  $^{155}\text{Dy}$  ( $T_{1/2} = 9.9$  h) represents the sum of the direct and indirect production through the decay of  $^{155}\text{Ho}$  ( $T_{1/2} = 48$  min). The agreement with the results of the three codes is acceptable. (Fig. 7)

#### 4.1.7. Cross-sections for the $^{nat}\text{Dy}(d,x)^{161}\text{Tb}$ reaction

The  $^{161}\text{Tb}$  ( $T_{1/2} = 6.89$  d) is produced via direct (d,2pxn) reactions if we neglect the small contribution from  $^{161}\text{Gd}$  decay ( $T_{1/2} = 3.66$  min) produced with the (d,3pxn) reaction. Our experimental data above 30 MeV are systematically higher than the theoretical results and the bump predicted by EMPIRE is not reproduced by the experiment (Fig. 8).

#### 4.1.8. Cross-sections for the $^{nat}\text{Dy}(d,x)^{160}\text{Tb}$ reaction

The radionuclide  $^{160}\text{Tb}$  ( $T_{1/2} = 72.3$  d) can only be produced directly by (d,2pxn) reactions as decay contribu-

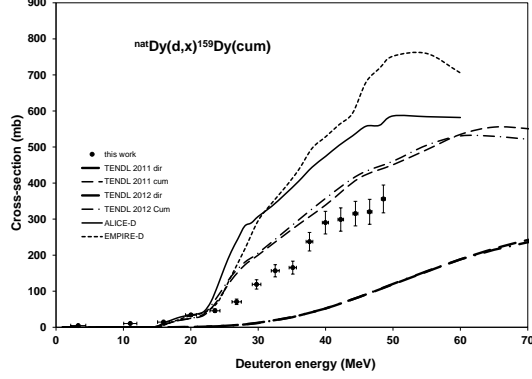


Figure 5: Experimental and theoretical excitation functions for  $^{nat}\text{Dy}(d,x)^{159}\text{Dy}(\text{cum})$

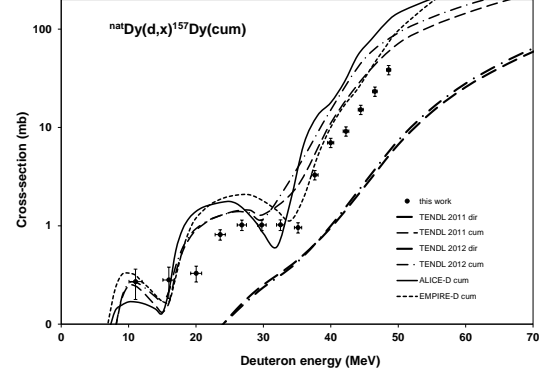


Figure 6: Experimental and theoretical excitation functions for  $^{nat}\text{Dy}(d,x)^{157}\text{Dy}(\text{cum})$

tions are closed from both sides. The activation cross-sections are shown in Fig. 9. There are significant disagreements with the results of the theoretical codes.

#### 4.1.9. Cross-sections for the $^{nat}\text{Dy}(d,x)^{156}\text{Tb}(\text{cum})$ reaction

The production cross-sections of  $^{156}\text{Tb}$  (Fig. 10) represent total activation cross-sections of the ground state: i.e. cumulative cross-section of the ground state after the decay of the two isomeric states ( $^{156m1}\text{Tb}$ , IT: 100 %,  $T_{1/2} = 3$  h and  $^{156m2}\text{Tb}$ , IT: 100 %,  $T_{1/2} = 24.4$  h). Large divergences can be seen between the different codes and the experimental results.

#### 4.1.10. Cross-sections for the $^{nat}\text{Dy}(d,x)^{155}\text{Tb}(\text{cum})$ reaction

The cross-sections for  $^{155}\text{Tb}$  ( $T_{1/2} = 5.32$  d) production are cumulative. They were determined from the spectra measured after the decay of progenitor  $^{155}\text{Ho}$  ( $T_{1/2} = 48$  min) and  $^{155}\text{Dy}$  ( $T_{1/2} = 9.9$  h) isotopes. The best description is given by the TENDL calculations, while up to 35 MeV the ALICE-D is also acceptable (Fig. 11).

#### 4.2. Integral yields

We calculated the integral yields for all investigated radionuclides from a spline fit to our experimental data.

The yields represent so called physical yields for instantaneous irradiation. No data for directly measured thick target yields were found in the literature. The yields are presented in Figs. 12 and 13. In Fig. 13 the most interesting isotopes are the  $^{161}\text{Ho}$  and  $^{162m}\text{Ho}$ , as they have also medical interest (Trknyi et al., 2013). The  $^{165g}\text{Dy}$  production yield is with an order of magnitude lower than that of the above two. Another group is formed from the remaining dysprosium isotopes i.e.  $^{159,157,155}\text{Dy}$ , which have much lower yield. In Fig. 13 the terbium radio-isotopes are presented. From the point of view of yield they rather belong to the latter group of the preceding figure.

## 5. Summary and conclusions

In the frame of systematic investigation of excitation functions of deuteron induced nuclear reactions, activation cross-sections on dysprosium were investigated up to 50 MeV. Independent or cumulative cross-sections for the formation of the radionuclides  $^{162m,161}\text{Ho}$ ,  $^{165,159,157,155}\text{Dy}$  and  $^{161,160,156,155}\text{Tb}$  through  $^{nat}\text{Dy}(d,x)$  nuclear reactions were measured for the first time. The experimental data were compared with the theoretical data obtained by the EMPIRE-D and the ALICE-IPPE-D codes and the TALYS data in TENDL library. The prediction of the codes differs significantly from each other, and from the

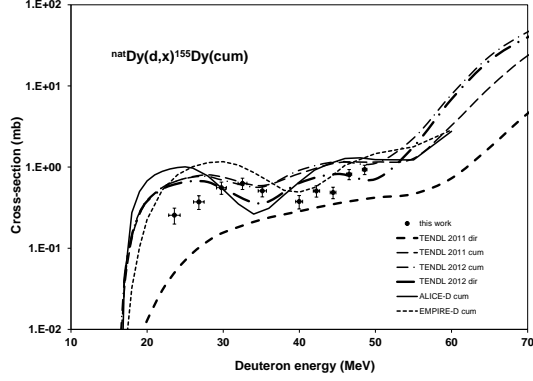


Figure 7: Experimental and theoretical excitation functions for  $^{nat}\text{Dy}(\text{d},\text{x})^{155}\text{Dy}(\text{cum})$

experimental data. In the case of EMPIRE-D and ALICE-D the phenomenological systematics improved but not solved all the disagreements. In the case of deuteron induced reactions there are still no significant improvements between the different TENDL versions. The (d,p) results of the TALYS code in TENDL are still largely discrepant. The new experimental data are therefore very important, to complete experimental activation database of deuteron induced reactions and for further improvement of theoretical models. As it was mentioned, the dysprosium is an important technological material, therefore the measured activation cross-sections can be useful in the field of medical isotope production and to estimate the radiation dose of caused by primer or secondary deuterons in reactors, accelerators and in space applications.

## 6. Acknowledgements

This work was performed in the frame of the HAS-FWO Vlaanderen (Hungary-Belgium) project. The authors acknowledge the support of the research project and of the respective institutions. We are grateful to all the authorities concerned. We thank to the Cyclotron Laboratory of the Universit Catholique in Louvain la Neuve (LLN) providing the beam time and the staff of the LLN Cyclone 90 cyclotron for performing the irradiations

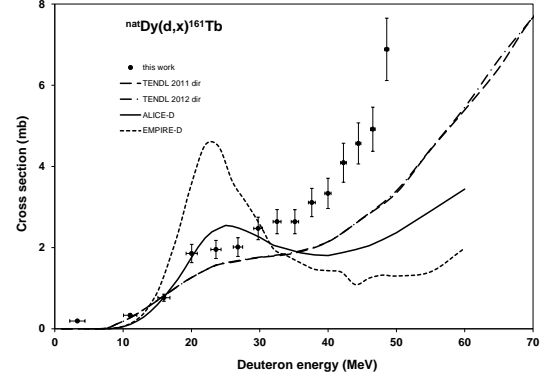


Figure 8: Experimental and theoretical excitation functions for  $^{nat}\text{Dy}(\text{d},\text{x})^{161}\text{Tb}$

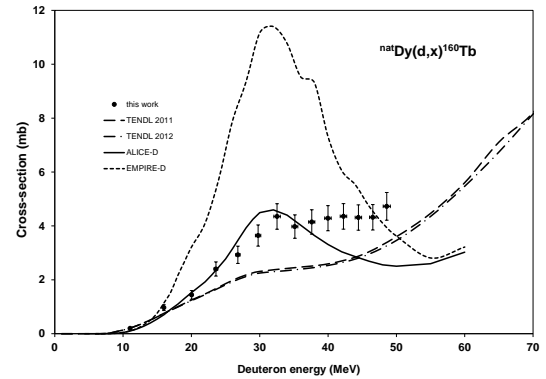


Figure 9: Experimental and theoretical excitation functions for  $^{nat}\text{Dy}(\text{d},\text{x})^{160}\text{Tb}$

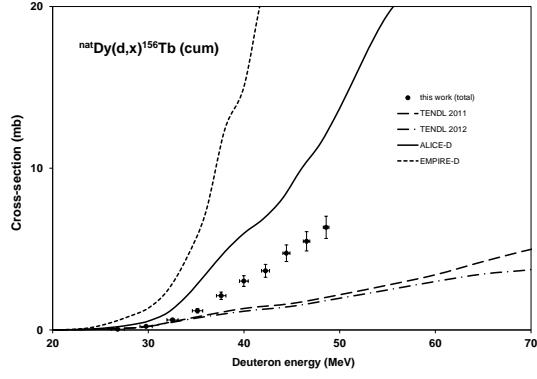


Figure 10: Experimental and theoretical excitation functions for  $^{nat}\text{Dy}(d,x)^{156}\text{Tb}(\text{cum})$

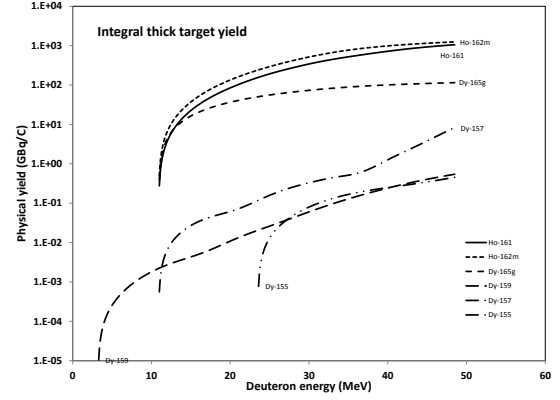


Figure 12: Integral yields as a function of proton energy for the production of  $^{162m,161}\text{Ho}$ ,  $^{165,159,157,155}\text{Dy}$  radioisotopes

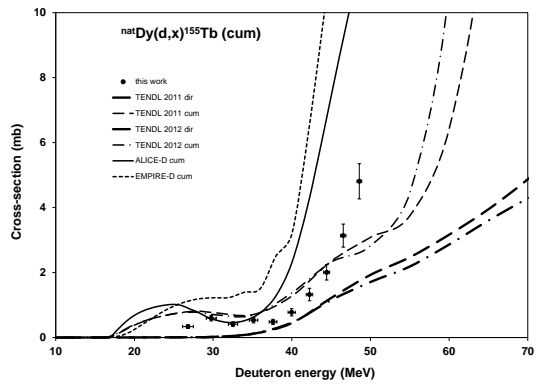


Figure 11: Experimental and theoretical excitation functions for  $^{nat}\text{Dy}(d,x)^{155}\text{Tb}(\text{cum})$

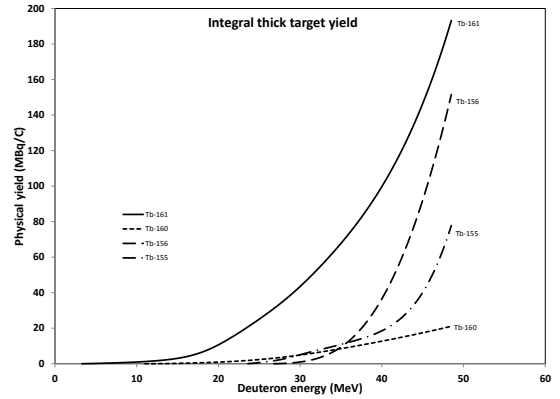


Figure 13: Integral yields as a function of proton energy for the production of  $^{161,160,156,155}\text{Tb}$  radioisotopes.

Table 2: Decay data and contributing reactions

Nuclide	Half-life	$E_\gamma$ (keV)	$I_\gamma$ (%)	Contributing reaction	Q-value (keV)
$^{162m}\text{Ho}$ IT: 62 %	67.0 min	57.74	4.4	$^{161}\text{Dy}(\text{d},\text{n})$ $^{162}\text{Dy}(\text{d},2\text{n})$ $^{163}\text{Dy}(\text{d},3\text{n})$ $^{164}\text{Dy}(\text{d},4\text{n})$	3050.38 -5146.61 -11417.62
$^{161}\text{Ho}$ $\varepsilon$ : 100 %	2.48 h	77.42 103.05 157.26 175.42	1.9 103.05 0.49 0.43	$^{160}\text{Dy}(\text{d},\text{n})$ $^{161}\text{Dy}(\text{d},2\text{n})$ $^{162}\text{Dy}(\text{d},3\text{n})$ $^{163}\text{Dy}(\text{d},4\text{n})$ $^{164}\text{Dy}(\text{d},5\text{n})$	2589.18 -3865.2 -12062.2 -18333.21 -25991.33
$^{155}\text{Ho}$ $\varepsilon + \beta^+$	48 min	103.89 136.30 240.19 325.40	2.17 5.00 12.5 2.75	$^{158}\text{Dy}(\text{d},5\text{n})$ $^{160}\text{Dy}(\text{d},7\text{n})$ $^{161}\text{Dy}(\text{d},8\text{n})$ $^{162}\text{Dy}(\text{d},9\text{n})$ $^{163}\text{Dy}(\text{d},10\text{n})$ $^{164}\text{Dy}(\text{d},11\text{n})$	-31593.3 -47001.9 -53456.3 -61653.3 ? ?
$^{165}\text{Dy}$ $\beta^-$ : 100 %	2.334 h	94.700 279.763 361.68 633.415 715.328	3.80 0.534 0.904 0.613 0.578	$^{164}\text{Dy}(\text{d},\text{p})$	3491.394
$^{159}\text{Dy}$ $\varepsilon$ : 100 %	144.4 d	58.0	2.27	$^{158}\text{Dy}(\text{d},\text{p})$ $^{160}\text{Dy}(\text{d},\text{p}2\text{n})$ $^{161}\text{Dy}(\text{d},\text{p}3\text{n})$ $^{162}\text{Dy}(\text{d},\text{p}4\text{n})$ $^{163}\text{Dy}(\text{d},\text{p}5\text{n})$ $^{164}\text{Dy}(\text{d},\text{p}6\text{n})$ $^{159}\text{Ho}$ decay	4608.11 -10800.48 -17254.87 -25451.86 -31722.87 -39380.99
$^{157}\text{Dy}$ $\varepsilon$ : 100 %	8.14 h	182.424 326.336	1.33 93	$^{158}\text{Dy}(\text{d},\text{p}2\text{n})$ $^{160}\text{Dy}(\text{d},\text{p}4\text{n})$ $^{161}\text{Dy}(\text{d},\text{p}5\text{n})$ $^{162}\text{Dy}(\text{d},\text{p}6\text{n})$ $^{163}\text{Dy}(\text{d},\text{p}7\text{n})$ $^{164}\text{Dy}(\text{d},\text{p}8\text{n})$ $^{157}\text{Ho}$ decay	-11280.12 -26688.71 -33143.1 -41340.09 -47611.11 -55269.23
$^{155}\text{Dy}$ $\varepsilon$ : 100 %	9.9 h	184.564 226.918	3.37 68.4	$^{158}\text{Dy}(\text{d},\text{p}4\text{n})$ $^{160}\text{Dy}(\text{d},\text{p}6\text{n})$ $^{161}\text{Dy}(\text{d},\text{p}7\text{n})$ $^{162}\text{Dy}(\text{d},\text{p}8\text{n})$ $^{163}\text{Dy}(\text{d},\text{p}9\text{n})$ $^{164}\text{Dy}(\text{d},\text{p}10\text{n})$ $^{155}\text{Ho}$ decay	-27690.7 -43099.3 -49553.7 -57750.7 -64021.7
$^{161}\text{Tb}$ $\beta^-$ : 100 %	6.89 d	74.56669 87.941 103.065 106.113 292.401	10.2 0.183 0.101 0.078 0.058	$^{161}\text{Dy}(\text{d},2\text{p})$ $^{162}\text{Dy}(\text{d},2\text{pn})$ $^{163}\text{Dy}(\text{d},2\text{p}2\text{n})$ $^{164}\text{Dy}(\text{d},2\text{p}3\text{n})$	-2035.16 -10232.16 -16503.17 -24161.29
$^{160}\text{Tb}$ $\beta^-$ : 100 %	72.3 d	86.7877 298.5783 879.378 966.166 1177.954	13.2 26.1 30.1 25.1 14.9	$^{160}\text{Dy}(\text{d},2\text{p})$ $^{161}\text{Dy}(\text{d},2\text{pn})$ $^{162}\text{Dy}(\text{d},2\text{p}2\text{n})$ $^{163}\text{Dy}(\text{d},2\text{p}3\text{n})$ $^{164}\text{Dy}(\text{d},2\text{p}4\text{n})$	-3277.34 -9731.73 -17928.73 -24199.74 -31857.86
$^{156}\text{Tb}$ $\varepsilon$ : 100 %	5.35 d	88.97 199.19 262.54 296.49 356.38 422.34 534.29 1065.11 1154.07 1222.44	18 41 5.8 4.5 13.6 8.0 67 10.8 10.4 31	$^{158}\text{Dy}(\text{d},2\text{p}2\text{n})$ $^{160}\text{Dy}(\text{d},2\text{p}4\text{n})$ $^{161}\text{Dy}(\text{d},2\text{p}5\text{n})$ $^{162}\text{Dy}(\text{d},2\text{p}6\text{n})$ $^{163}\text{Dy}(\text{d},2\text{p}7\text{n})$ $^{164}\text{Dy}(\text{d},2\text{p}8\text{n})$	-17899.45 -33308.04 -39762.43 -47959.42 -54230.44 -61888.55
$^{155}\text{Tb}$ $\varepsilon$ : 100 %	5.32 d	86.55 105.318 148.64 161.29 163.28 180.08 262.27	32.0 25.1 2.65 2.76 4.44 7.5 5.3	$^{158}\text{Dy}(\text{d},2\text{p}3\text{n})$ $^{160}\text{Dy}(\text{d},2\text{p}5\text{n})$ $^{161}\text{Dy}(\text{d},2\text{p}6\text{n})$ $^{162}\text{Dy}(\text{d},2\text{p}7\text{n})$ $^{163}\text{Dy}(\text{d},2\text{p}8\text{n})$ $^{155}\text{Dy}$ decay	-24813.9 -40222.5 -46676.9 -54873.9 -61144.9

Naturally occurring dysprosium is composed of 7 isotopes ( $^{156}\text{Dy}$ -0.06 %,  $^{158}\text{Dy}$ -0.10 %,  $^{160}\text{Dy}$ -2.34 %,  $^{161}\text{Dy}$ -18.9 %,  $^{162}\text{Dy}$ -25.5 %,  $^{163}\text{Dy}$ -24.9 % and  $^{164}\text{Dy}$ -28.2 %). When complex particles are emitted instead of individual protons and neutrons the Q-values have to be decreased by the respective binding energies of the compound particles: np-d, +2.2 MeV; 2np-t, +8.48 MeV; n2p- $^3\text{He}$ , +7.72 MeV; 2n2p-a, +28.30 MeV



Table 3: Experimental cross-sections of  $^{nat}\text{Dy}(\text{d},\text{x})^{162m}\text{Ho}$ ,  $^{161g}\text{Ho}(\text{m}+)$ ,  $^{165g}\text{Dy}(\text{m}+)$ ,  $^{159}\text{Dy}(\text{cum})$ ,  $^{157}\text{Dy}(\text{cum})$ ,  $^{155}\text{Dy}(\text{cum})$  reactions

E $\pm \Delta E$ (MeV)		Cross-section( $\sigma$ ) $\pm \Delta\sigma$ (mb)											
		$^{162m}\text{Ho}$		$^{161g}\text{Ho}$		$^{165g}\text{Dy}$		$^{159}\text{Dy}$		$^{157}\text{Dy}$		$^{155}\text{Dy}$	
3.3	1.1							4.8	0.5				
11.0	1.0	36.6	4.2	45.0	5.5	58.0	6.4	10.4	1.1	0.3	0.1		
16.0	0.9	91.7	10.1	127.5	14.7	56.6	6.2	14.4	1.6	0.3	0.1		
20.0	0.8	126.1	13.9	181.0	20.5	40.4	4.6	34.2	3.7	0.3	0.1		
23.6	0.7	147.5	16.3	234.9	26.3	32.8	3.8	45.9	5.0	0.8	0.1	0.3	0.1
26.8	0.7	172.8	19.0	250.9	28.3	27.5	3.4	70.6	7.6	1.0	0.1	0.4	0.1
29.8	0.6	189.9	20.8	295.1	33.1	26.9	3.3	118.9	12.9	1.0	0.1	0.6	0.1
32.5	0.6	192.5	21.1	277.7	31.3	25.9	3.1	156.7	17.0	1.0	0.1	0.6	0.1
35.1	0.5	166.8	18.4	265.8	29.8	20.1	2.7	165.4	17.9	1.0	0.1	0.5	0.1
37.6	0.5	143.2	15.7	301.0	33.7	18.6	2.4	237.5	25.7	3.3	0.4		
40.0	0.5	106.1	12.5	274.8	31.3	10.5	1.9	290.3	31.4	7.0	0.8	0.4	0.1
42.3	0.4	93.9	10.8	295.2	33.1	10.3	1.7	298.8	32.3	9.1	1.0	0.5	0.1
44.4	0.4	94.4	11.2	242.0	28.1	9.6	2.0	315.3	34.1	15.2	1.6	0.5	0.1
46.5	0.3	75.2	10.0	222.2	26.9	8.8	3.0	320.3	34.7	23.2	2.5	0.8	0.1
48.6	0.3	66.7	9.0	219.9	26.6	10.0	2.6	356.0	38.5	38.5	4.2	0.9	0.1

Table 4: Experimental cross-sections of  $^{nat}\text{Dy}(\text{d},\text{x})^{161}\text{Tb}$ ,  $^{160}\text{Tb}$ ,  $^{156}\text{Tb}(\text{cum})$ ,  $^{155}\text{Tb}(\text{cum})$  reactions

E $\pm \Delta E$ (MeV)		Cross-section( $\sigma$ ) $\pm \Delta\sigma$ (mb)							
		$^{161}\text{Tb}$		$^{160}\text{Tb}$		$^{156}\text{Tb}$		$^{155}\text{Tb}$	
3.3	1.1	0.19	0.02						
11.0	1.0	0.3	0.01	0.20	0.02				
16.0	0.9	0.8	0.1	1.0	0.1				
20.0	0.8	1.9	0.2	1.4	0.2				
23.6	0.7	2.0	0.2	2.4	0.3			0.2	0.01
26.8	0.7	2.0	0.2	2.9	0.3	0.04	0.01	0.3	0.1
29.8	0.6	2.5	0.3	3.6	0.4	0.22	0.03	0.6	0.1
32.5	0.6	2.6	0.3	4.4	0.5	0.6	0.1	0.4	0.1
35.1	0.5	2.6	0.3	4.0	0.4	1.2	0.1	0.5	0.1
37.6	0.5	3.1	0.3	4.1	0.5	2.1	0.2	0.5	0.1
40.0	0.5	3.3	0.4	4.3	0.5	3.0	0.3	0.8	0.1
42.3	0.4	4.1	0.5	4.4	0.5	3.7	0.4	1.3	0.2
44.4	0.4	4.6	0.5	4.3	0.5	4.7	0.5	2.0	0.2
46.5	0.3	4.9	0.5	4.3	0.5	5.5	0.6	3.1	0.4
48.6	0.3	6.9	0.8	4.7	0.5	6.3	0.7	4.8	0.5

## References

- Andersen, H. H., Ziegler, J. F., 1977. Hydrogen stopping powers and ranges in all elements. The Stopping and ranges of ions in matter, Volume 3. The Stopping and ranges of ions in matter. Pergamon Press, New York.
- Bonardi, M., 1987. The contribution to nuclear data for biomedical radioisotope production from the milan cyclotron facility.
- Canberra, 2000. [http://www.canberra.com/products/radio-chemistry\\_lab/genie-2000-software.asp](http://www.canberra.com/products/radio-chemistry_lab/genie-2000-software.asp).
- Dityuk, A. I., Konobeyev, A. Y., Lunev, V. P., Shubin, Y. N., 1998. New version of the advanced computer code alice-ippe. Tech. rep., IAEA.
- Habs, D., Köster, U., 2012. Production of medical radioisotopes with high specific activity in photonuclear reactions with  $\gamma$ -beams of high intensity and large brilliance. *Applied Physics B* 103 (2), 501–519.
- Herman, M., Capote, R., Carlson, B. V., Oblozinsky, P., Sin, M., Trkov, A., Wienke, H., Zerkin, V., 2007. Empire: Nuclear reaction model code system for data evaluation. *Nuclear Data Sheets* 108 (12), 2655–2715.
- Ignatyuk, A. V., 2011. Phenomenological systematics of the (d,p) cross sections, [http://www-nds.iaea.org/fendl3/000pages/rcm3/slides/ignatyuk\\_fendl-3](http://www-nds.iaea.org/fendl3/000pages/rcm3/slides/ignatyuk_fendl-3)
- Kannan, U., Ganesan, S., 2010. Dysprosium as a resonance absorber and its effect on the coolant void reactivity in advanced heavy water reactor (ahwr). *Annals of Nuclear Energy* 37 (2), 270–276.
- Kinsey, R. R., Dunford, C. L., Tuli, J. K., Burrows, T. W., 2010. Nudat 2.6. In: *Proceedings of the 9th International Symposium on Capture Gamma Ray Spectroscopy and Related Topics*. Vol. 2. Springer Hungarica Ltd, p. 657.
- Koning, A. J., Hilaire, S., Duijvestijn, M. C., 2007. Talys-1.0.
- Koning, A. J., Rochman, D., van der Marck, S., Kopecky, J., Sublet, J. C., Pomp, S., Sjostrand, H., Forrest, R., Bauge, E., Henriksen, H., 2012. Tendl-2012: Talys-based evaluated nuclear data library.
- of-Weights-and Measures, I.-B., 1993. Guide to the expression of uncertainty in measurement, 1st Edition. International Organization for Standardization, Geneva, Switzerland.
- Pritychenko, B., Sonzogni, A., 2003. Q-value calculator.
- Rao, D. V., Govelitz, G. F., Sastry, K. S., 1977. Dysprosium-159 for transmission imaging and bone mineral analysis. *Medical Physics* 4 (2), 109–14.
- Srivastava, S. C., 2004. Treatment of bone and joint pain with electron emitting radiopharmaceuticals. *Indian Journal of Nuclear Medicine* 19 (3), 89–97.
- Székely, G., 1985. Fgm - a flexible gamma-spectrum analysis program for a small computer. *Computer Physics Communications* 34 (3), 313–324.
- Takacs, S., Tarkanyi, F., Hermanne, A., Rebeles, R. A., 2011. Activation cross sections of proton induced nuclear reactions on natural hafnium. *Nuclear Instruments & Methods in Physics Research Section B-Beam Interactions with Materials and Atoms* 269 (23), 2824–2834.
- Tarkanyi, F., Ditroi, F., Hermanne, A., Takacs, S., Ignatyuk, A. V., 2013. Investigation of production routes for the  $^{161}\text{Ho}$  auger-electron emitting radiolanthanide, a candidate for therapy. *Journal of Radioanalytical and Nuclear Chemistry* 298, 277–286.
- Tarkanyi, F., Ditroi, F., Takacs, S., Király, B., Hermanne, A., Sonck, M., Baba, M., Ignatyuk, A. V., 2012. Investigation of activation cross-sections of deuteron induced nuclear reactions on natmo up to 50 mev. *Nuclear Instruments & Methods in Physics Research Section B-Beam Interactions with Materials and Atoms* 274, 1–25.
- Tarkanyi, F., Szelecsényi, F., Takacs, S., 1991. Determination of effective bombarding energies and fluxes using improved stacked-foil technique. *Acta Radiologica, Supplementum* 376, 72.
- Tarkanyi, F., Takacs, S., Gul, K., Hermanne, A., Mustafa, M. G., Nortier, M., Oblozinsky, P., Qaim, S. M., Scholten, B., Shubin, Y. N., Youxiang, Z., 2001. Beam

monitor reactions (chapter 4). charged particle cross-section database for medical radioisotope production: diagnostic radioisotopes and monitor reactions. Tech. rep., IAEA.